Two-dimensional control of surface plasmons and directional beaming from arrays of subwavelength apertures

D. Egorov,[1,2] B. S. Dennis,[1] and G. Blumberg[1,*]
[1]*Bell Laboratories, Lucent Technologies, Murray Hill, New Jersey 07974, USA*
[2]*Department of Physics, Harvard University, Cambridge, Massachusetts 02138, USA*

M. I. Haftel
Center for Computational Materials Science, Naval Research Laboratory, Washington, DC 20375, USA
(Received 30 June 2003; revised manuscript received 5 March 2004; published 23 July 2004)

We demonstrate two-dimensional control of coherent modes of surface plasmons (SP) in a metallic array of subwavelength apertures. SP mode intensity and propagation direction is manipulated by varying the wavelength, incidence angle, and polarization of the excitation photons. We also demonstrate directional beaming of light from this device. Finite-difference-time-domain simulations of the SP modes closely resemble the observations by near-field scanning optical microscopy. Calculated SP coupling efficiencies and transmission are also presented.

DOI: 10.1103/PhysRevB.70.033404 PACS number(s): 78.67.−n, 73.20.Mf, 78.20.Ci

Recent works on extraordinary optical transmission[1,2] and light beaming[3] in sub-wavelength periodically structured metal films suggest a direction for fabricating optical devices that operate below the diffraction limit and utilize the coherent fluctuations of surface bound electron charges known as surface plasmons (SP). Significant advances in this area may be possible if SPs can be controllably converted to and from free-space photons, and if their surface propagation can be intentionally directed in two dimensions (2D).

Control of SPs can be achieved through adjustment of the excitation parameters, periodicity of the structure, and dielectric properties of the interface, so that a resonant coupling condition results in propagation in a given direction [Fig. 1(b)]. For a metal-dielectric interface the frequency of SP oscillations is tied to the wave vector $\mathbf{k}^{SP}$ by $k^{SP}=\omega/c\sqrt{(\epsilon_m(\omega)\cdot\epsilon_d)/(\epsilon_m(\omega)+\epsilon_d)}$, where $\epsilon_m(\omega)$ and ϵ_d are the dielectric functions of the metal and dielectric.[4] For photons in a dielectric $k_x^0=\omega/c\sqrt{\epsilon_d}\sin\theta$, where $k_x^0=2\pi/\lambda\sin\theta$ is the in-plane component with wavelength λ and incidence angle θ [Fig. 2(a)]. If a 2D periodic array of apertures is introduced, conservation of energy and quasimomentum can be satisfied if $\mathbf{k}^{SP}=\mathbf{k}_x^0\pm m\mathbf{G}_x\pm n\mathbf{G}_y$, where $G_i=2\pi/a_i$ $(i=1,2)$. This condition determines the allowed SP modes denoted here as $(m;n)$ [Fig. 1].

In this Report, we demonstrate that SPs can form coherent modes whose intensity and 2D propagation direction can be manipulated by varying the wavelength, incidence angle, and polarization of the excitation light. We also demonstrate the reverse conversion of SPs back into light and observe directional beaming. We apply the finite-difference-time-domain (FDTD) method to simulate the electromagnetic fields produced in this experiment. The simulations bear close resemblance to the observations with the propagation of SP modes apparent.

To image the SP modes we employ a near-field scanning optical microscope (NSOM-100 by Nanonics Imaging Ltd., Jerusalem, Isreal) [Fig. 2(a)]. The sample, a gold film on a fused silica substrate with an array of subwavelength apertures, rests on a *XYZ* piezoscanning stage, and is illuminated from below with a Ti:Sapphire laser. The expanded 10 mm wide laser beam is focused with a 300 mm lens on to the array of holes, resulting in a 2^0 spread in the incidence angle (wavelength resonance broadens by about 10 nm). A NSOM fiber tip (no metallic coating) is maintained in contact with the sample. Since the tip is within the decay length of the evanescent SP field, the field can be converted into light that propagates down the fiber.[5] The photon counting rate is then the measure of the evanescent field strength at the metal surface. Figure 2(b) shows a surface plot of the field intensity distribution over the gold film when the resonant excitation condition
$(-2;0)$ is met. A long straight SP mode emerges from the hole array in agreement with this resonance. Also shown is the exponential decay of this mode. The data is the intensity integrated over the width of the mode. The fit (solid line)

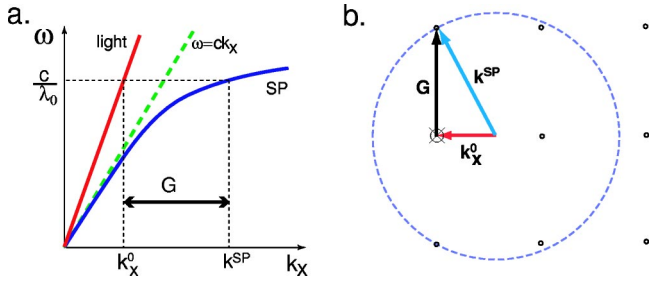

FIG. 1. (Color online) (a) Dispersion curves for SPs and photons (light) with k_x^0. The dashed line represents the limiting case for photons, $\theta=90^0$, which has maximum in-plane momentum. The periodic structure of the nanoarray allows excitation of SPs when the momentum difference is equal to an integer multiple of **G**. (b) In two dimensions, SPs can be excited in a given direction by appropriately selecting the frequency ω and angle θ of incident light. The crossed circle represents the origin of the reciprocal lattice and small circles represent the vertices. Excitation occurs when $\mathbf{k}^{SP}$ can connect the origin of $\mathbf{k}_x^0$ with one of the reciprocal lattice vertices, i.e., when the dashed circle crosses a vertex.

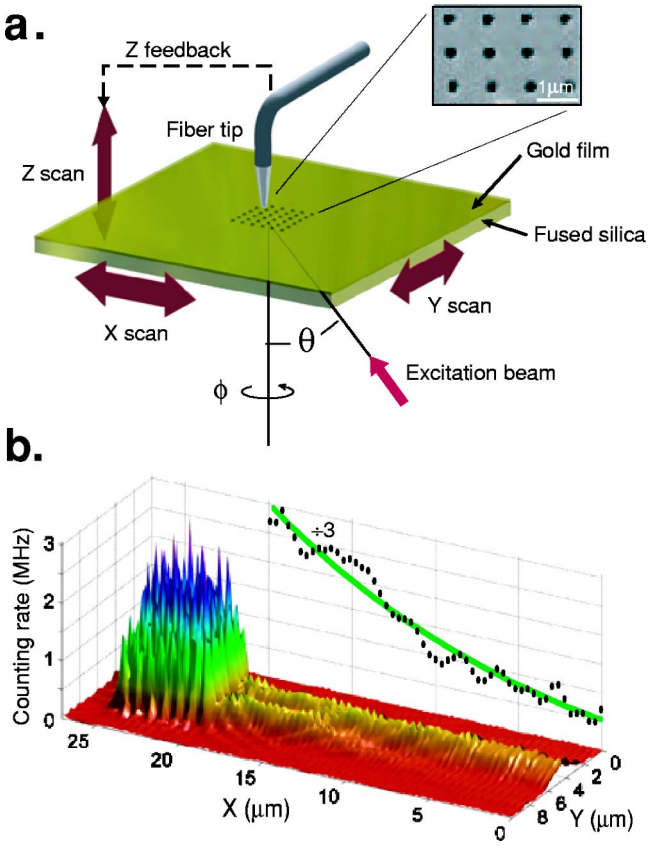

FIG. 2. (Color online) (a) The sample rests on top of the NSOM piezostage. Laser wavelength, angle, and polarization can be varied to achieve 2D control over SPs. The hole array consists of periodic perforations created by a focused ion beam in a 150 nm Au film deposited onto a transparent 0.16 mm thick fused silica substrate with a 5 nm adhesion layer of Ti. Inset: SEM image of a section of the 6×7 array of ~200 nm holes (a_x=840 and a_y=950 nm). SP intensity on the Au surface is measured by counting photons that couple into a 200-nm-aperture optical fiber. (b) NSOM image demonstrating a SP mode created by a nanoarray. The region of high intensity corresponds to photons from the array of holes. Excitation wavelength λ=760 nm, incidence angle θ=50°; coupling condition is $(-2;0)$. Also shown is the intensity integrated over the width of the mode with an exponential fit (decay length 19±2 μm) (Ref. 7).

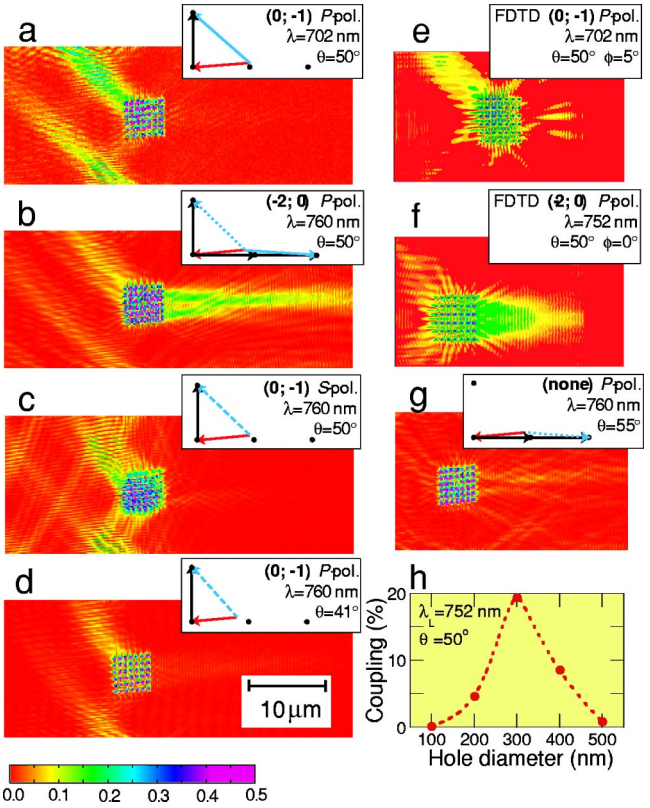

FIG. 3. (Color online) 2D control of SP modes is achieved by varying the laser wavelength λ [(a) versus (b)], incidence angle θ [(b) versus (d) versus (g)], or polarization [(b) versus (c)]. Vector diagrams represent calculated wave-vector coupling conditions with $\mathbf{k}^{SP}$ [light gray (blue online)], $\mathbf{k}_x^0$ [dark gray (red online)], and $\mathbf{G}$ (black). Solid, dashed, and dotted lines represent decreasing SP mode intensity. Images are normalized by their peak intensity and saturated 50%. The sample is rotated by $\phi=5^\circ$ to eliminate symmetrical coupling conditions. SP modes coming from the lower parts of images are from nearby arrays on the same sample. (e) and (f) represent 2D cuts, taken 50 nm above the surface, of calculated FDTD field intensities after 53 and 63 fs propagation time, respectively. (h) shows SP coupling efficiencies [same conditions as (f)] predicted by FDTD calculations as a function of array hole diameter.

gives a decay length of 19±2 μm with a background of 8% of the maximum signal. The background may be due to a free space beam parallel to the surface and oscillations due to interference with the SP.

We model the electromagnetic fields by the FDTD method. The code used here employs a nonstandard finite difference (NSFD) algorithm[8,9] that is similar to the Yee algorithm[10] but with more accuracy on a coarse ($\sim\lambda/10$) grid.[11] The Yee and the NSFD algorithms were modified for stability for negative ϵ and positive conductivity σ encountered for SP frequencies.[12] The heart of the method is to replace in the regions of negative ϵ the Maxwell curl equation for H with its frequency domain analog (i.e., $\partial\mathbf{E}/\partial t \rightarrow -i\omega\mathbf{E}$), but retain the time-dependent form of the curl equation for $\mathbf{E}$ as well as the time stepping features of the Yee algorithm.[10] To retain the time-updating feature of the curl equation for H, a second-order accurate extrapolation of H at the current time from the values at the two previous time steps of the curl $\mathbf{E}$ equation is used. The simulations are carried out at fixed frequencies, either corresponding to the wavelengths examined in this experiment or those where the SP modes are resonant. An incident wave is turned on over ten periods, and the simulation is run long enough for a steady-state solution to be developed (usually 10–20 additional periods). Mur absorbing boundary conditions are employed, and the incident-wave-scattered wave formalism described by Taflove[13] is used. Since the field transmission is relatively small above the metal, the reflected field from the numerical boundary is very small and does not affect the simulation of SPs. In the present calculation we use a uniform spatial grid with $\Delta x=\Delta y=\Delta z=50$ nm. The time step is $\Delta t=\tau/120$, where τ is the period, which is sufficient for numerical stability and fields that are accurate to the 2–5 % level.

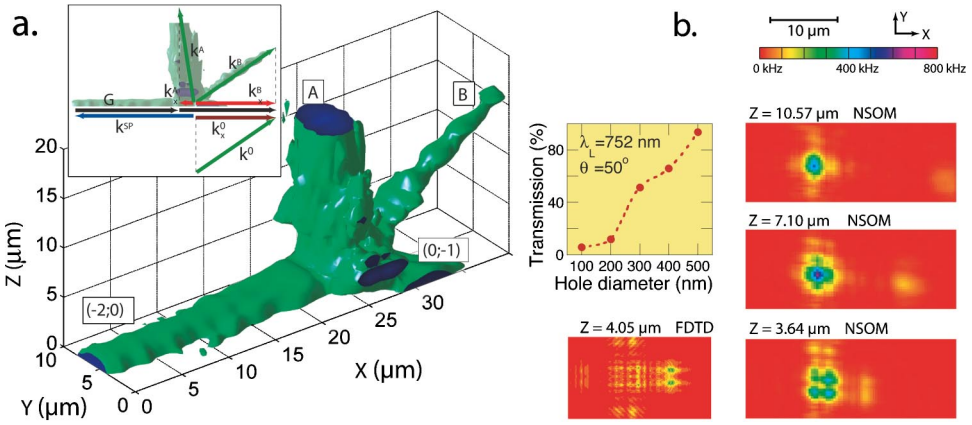

FIG. 4. (Color online) Conversion of SPs into free-space photons [conditions as in Fig. 3(b)]. (a) Surface of constant light intensity in the space above the array. The tip is held at constant Z positions for XY scans. The isosurface shown corresponds to a photon counting rate of 46 kHz. The laser beam illuminating the sample from the negative Z side excites SPs via array coupling. Two SP modes, $(0;-1)$ and $(-2;0)$, run along the air-gold interface; their evanescent fields are confined to a small volume above the surface. Two propagating beams, labeled A and B, emerge out of the array as SPs are converted back into photons via array coupling. Inset: illustration of in-coupling and out-coupling conditions. SP mode $(-2;0)$ is produced when $\mathbf{k}^{SP}=\mathbf{k}_x^0+2\mathbf{G}$. Light beams A and B have in-plane components of wave-vectors $\mathbf{k}_x^A=\mathbf{k}^{SP}+\mathbf{G}$ and $\mathbf{k}_x^B=\mathbf{k}^{SP}+2\mathbf{G}$, and absolute values of wave-vectors $k^A=k^B=2\pi/\lambda$. Data were not corrected for anisotropy from the tip's acceptance angle. (b) Three Z-cuts show beam A in the center and B moving to the right. Also from FDTD calculations a Z-cut of field intensity (after 38 fs propagation time) and light transmission versus hole diameter.

In this work we focus on varying the excitation parameters: θ,λ, and polarization. We keep the angle between the light incidence plane and array axis, ϕ [Fig. 2(a)], constant, although in principle it can be used as an additional parameter. Figures 3(a)–3(g) provide a demonstration of SP mode switching. Frame (b) has a pronounced straight $(-2;0)$ mode and a weaker, slightly off-resonance, diagonal $(0;-1)$ mode. By keeping θ constant and decreasing λ, we increase both k^{SP} and k_x^0 and are able to turn the $(-2;0)$ mode off and increase the strength of the $(0;-1)$ mode, as shown in frame (a). In frame (d), λ is kept fixed and θ is reduced, i.e., k_x^0 is decreased while k^{SP} remains constant, which turns off the straight mode while keeping the diagonal mode at nearly the same strength. Note that, as predicted by the coupling condition calculations, the angle of the $(0;-1)$ mode with respect to the X axis is modified compared to frames (a) and (b). By increasing θ, on the other hand, we can turn both modes off, as in frame (g). Finally, the polarization provides an additional parameter for SP control. If the incident laser polarization is rotated from p to s, then the momentum conservation condition does not change. However, the electric field vector $\mathbf{E}$ of the incident light is now perpendicular to the direction of propagation of the $(-2;0)$ mode. Since SPs are longitudinal electron density waves, excitation in the direction perpendicular to $\mathbf{E}$ does not occur, as in frame (c). Figure 3 demonstrates that by varying the excitation parameters in a fairly narrow interval we are able to turn SP modes on or off, or modify their strength and direction. It is important to note that SP mode switching is not limited to the cases illustrated here: Fig. 1(b) suggests a wide variety of possible switching configurations and exit angles. Such a degree of control is particular to 2D surface structures, and is not possible when SPs are excited using zero- or one-dimensional structures.[14,15]

Frames (e) and (f) of Fig. 3 give the calculated FDTD field intensities 50 nm above the surface for incident conditions comparable to those examined in (a) and (b) [$(0;-1)$ and $(-2;0)$ modes, respectively]. The calculations were carried out for free standing Au films. Frame (e) clearly shows the propagation of the $(0;-1)$ SP mode in the same direction as, and similar features to, the experimentally observed SP. We also simulated the fields for an unrotated sample at λ $=667$ nm, which, employing the measured dielectric constants,[6,7] should be the resonant frequency to create degenerate $(0;1)$ and $(0;-1)$ modes for a 50° incidence angle. Both of these modes are observed in the simulation, whereas the SP observations in frames (a) and (e) show the efficacy of altering the frequency and incidence conditions to select the $(0;-1)$ mode. The simulation in (f) is for an unrotated sample with $\lambda=752$ nm, which is the resonant frequency for $\theta=50°$ using the measured ϵ.[6] Again, the SP mode clearly appears, with its features, especially the convergence of two submodes about 10 μm after the nanoarray, resembling Figs. 2(b) and 3(b). The utility of the FDTD method in predicting and analyzing SP modes is thus confirmed. For the same conditions as in (f), frame (h) shows the SP coupling efficiency predicted by FDTD calculations as a function of hole diameter for arrays in a 150 nm thick Au film. The coupling efficiency is calculated by integrating the Poynting vector component in the direction of the SP propagation (x) over the normal (y-z) plane, and taking its ratio to the z component of the incident Poynting vector integrated over the area of the holes. Since this ratio varies with x, the efficiency plotted in Fig. 3(h) is the maximum in the region of the SP's—typically $1-2$ μm past the end of the array. When normalized to the area of the holes there is a resonant efficiency of almost 20% for diameter 300 nm at 50°. This type of maximum, attributed to Fabry-Pérot resonances, has also been seen in simulations of transmission through single holes.[16]

To fulfil the potential for miniaturization of optical devices, the details of the conversion of light to SP modes and

back to light again from structures designed for SP manipulation must be understood. To gain insight into the light intensity distribution near the surface, we set our scanning stage to hold the tip at a fixed height Z above the surface. By taking XY scans as a function of the tip height we are able to map out the volume distribution of light intensity above the array, as shown in Fig. 4. We observe two SP modes propagating along the surface, and two out-of-plane beams of light, labeled A and B. Since the apertures are too small to allow direct light transmission, we attribute the beams to SP-to-light conversion on the air-metal interface. Beam B emerges at an angle equal to the angle of incidence θ of the excitation laser, representing zero-order diffraction, i.e., the conversion condition that is identical to the plasmon excitation condition. Beam A is first-order diffracted, i.e., the conversion condition differs from the excitation condition by one **G**-vector. This measurement confirms the highly directional nature of free-space light from subwavelength apertures down to a few microns away from the surface, suggesting exciting possibilities in photonic device miniaturization.

The frame in Fig. 4(b) labeled FDTD gives the calculated results for a scan at 4.05 μm above the surface. The scan shows evidence of the A and B free-space beams and closely resembles the fine structure of the experimental scan. The transmission efficiency, also shown in Fig. 4(b), is calculated as in Fig. 3(h), except that the SP Poynting vector is replaced by the z-component of the Poynting vector and this is integrated over the x-y plane 2 μm above the film (above which this integrated quantity does not appreciably change). A resonance similar to that in Fig. 3(h) is seen at 300 nm hole diameter.

The method presented for 2D control of SP mode propagation directions and intensities is a step toward complex plasmon-based photonic devices. Combining it with other methods of adjusting light-plasmon coupling, such as coating the surface with a variable layer of dielectric,[17] liquid crystals,[18] or nonlinear optical material[19] may allow additional degrees of control of SP mode propagation using electronic and optical methods. Placing additional arrays on lines of SP mode propagation may allow localized, directional outcoupling of light at points away from the excitation spot; thus fast and complex microscale optical routers and switches may be constructed using simple focused-ion beam or lithographic fabrication techniques. Adding mirrors,[15,20] lenses,[15] beamsplitters, interferometers,[20] or plasmon waveguides[21] are other ways to guide SPs. In addition, the local density of electromagnetic energy in SP modes may be orders of magnitude greater than in the excitation laser beam, especially if the SP modes are focused using lenses or mirrors. These intense fields can be used for controlled spectroscopic surface-enhanced Raman scattering studies of single molecules,[22] and allow fabrication of highly sensitive chemical and biological sensors. As an inverse problem, SP diffraction can be used for recognition of periodic structures on surfaces.

*Electronic address: girsh@bell-labs.com

[1] T. W. Ebbesen, H. J. Lezec, H. F. Ghaemi, T. Thio, and P. A. Wolff, Nature (London) **391**, 667 (1998).
[2] E. Altewischer, M. P. van Exter, and J. P. Woerdman, Nature (London) **418**, 304 (2002).
[3] H. J. Lezec, A. Degiron, E. Devaux, R. A. Linke, L. Martin-Moreno, F. J. Garcia-Vidal, and T. W. Ebbesen, Science **297**, 820 (2002).
[4] H. Raether, *Surface Plasmons* (Springer, Berlin, 1988).
[5] Th. Huser, L. Novothy, Th. Lacoste, R. Eckert, and H. Heinzelmann, J. Opt. Soc. Am. A **16**, 141 (1999).
[6] P. B. Johnson and R. W. Christy, Phys. Rev. B **6**, 4370 (1972).
[7] Based on the dielectric constants (Ref. 6) for gold at 760 nm the calculated decay length is 38 μm.
[8] J. B. Cole, Comput. Phys. **8**, 730 (1994).
[9] J. B. Cole, IEEE Trans. Microwave Theory Tech. **45**, 991 (1997).
[10] K. S. Yee, IEEE Trans. Antennas Propag. **14**, 302 (1966).
[11] J. B. Cole, Comput. Phys. **12**, 82 (1998).
[12] M. I. Haftel, Bull. Am. Phys. Soc. **48**, 293 (2003).
[13] Allen Taflove, *Computational Electrodynamics, The Finite-Difference Time-Domain Method* (Artech House, Boston, 1995).
[14] H. Ditlbacher, J. R. Krenn, N. Felidj, B. Lamprecht, G. Schider, M. Salerno, A. Leitner, and F. R. Aussenegg, Appl. Phys. Lett. **80**, 404 (2002).
[15] I. I. Smolyaninov, D. L. Mazzoni, J. Mait, and C. C. Davis, Phys. Rev. B **56**, 1601 (1997).
[16] F. J. Garcia de Abajo, Opt. Express **10**, 1475 (2002).
[17] A. Krishnan, T. Thio, T. J. Kim, H. J. Lezec, T. W. Ebbesen, P. A. Wolff, J. Pendry, L. Martin-Moreno, and F. J. Garcia-Vidal, Opt. Commun. **200**, 1 (2001).
[18] T. J. Kim, T. Thio, T. W. Ebbesen, D. E. Grupp, and H. J. Lezec, Opt. Lett. **24**, 256 (1999).
[19] I. I. Smolyaninov, A. V. Zayats, A. Gungor, and C. C. Davis, Phys. Rev. Lett. **88**, 187402 (2002).
[20] H. Ditlbacher, J. R. Krenn, G. Schider, A. Leitner, and F. R. Aussenegg, Appl. Phys. Lett. **81**, 1762 (2002).
[21] S. A. Maier, M. L. Brongersma, P. G. Kik, S. Meltzer, A. A. G. Requicha, and H. A. Atwater, Adv. Mater. (Weinheim, Ger.) **13**, 1501 (2001).
[22] H. Xu, E. J. Bjerneld, M. Käll, and L. Börjesson, Phys. Rev. Lett. **83**, 4357 (1999).